Neuron, Vol. 5, 433–443, October, 1990, Copyright © 1990 by Cell Press

Alteration and Restoration of K^+ Channel Function by Deletions at the N- and C-Termini

Antonius M. J. VanDongen, Georges C. Frech, John A. Drewe, Rolf H. Joho, and Arthur M. Brown
Department of Molecular Physiology and Biophysics
Baylor College of Medicine
Houston, Texas 77030

Summary

Voltage-dependent ion channels are thought to consist of a highly conserved repeated core of six transmembrane segments, flanked by more variable cytoplasmic domains. Significant functional differences exist among related types of K^+ channels. These differences have been attributed to the variable domains, most prominently the N- and C-termini. We have therefore investigated the functional importance of both termini for the delayed rectifier K^+ channel from rat brain encoded by the *drk1* gene. This channel has an unusually long C-terminus. Deletions in either terminus affected both activation and inactivation, in some cases profoundly. Unexpectedly, more extensive deletions in both termini restored gating. We could therefore define a core region only slightly longer than the six transmembrane segments that is sufficient for the formation of channels with the kinetics of a delayed rectifier.

Introduction

Voltage-dependent ion channels are a diverse class of membrane proteins that form aqueous pores in the cell membrane. They are characterized by a steep voltage dependence of their opening behavior. Within this class there are large differences in kinetics, voltage dependence of activation and inactivation, and ion selectivity. The amino acid sequence of a growing number of Na^+, Ca^{2+}, and especially K^+ channels has been determined (Noda et al., 1984, 1986a; Baumann et al., 1987; Kamb et al., 1987, 1988; Papazian et al., 1987; Salkoff et al., 1987; Tanabe et al., 1987; Tempel et al., 1987, 1988; Auld et al., 1988; Baumann et al., 1988; Kayano et al., 1988; Schwarz et al., 1988; Butler et al., 1989; Christie et al., 1989; Frech et al., 1989; McKinnon, 1989; Mikami et al., 1989; Stühmer et al., 1989b; Trimmer et al., 1989; Yokoyama et al., 1989). Most of these channels have been expressed in Xenopus oocytes, confirming their identity, although detailed functional characterizations are still sparse (Noda et al., 1986b; Stühmer et al., 1987; Iverson et al., 1988; Timpe et al., 1988a; Leonard et al., 1989; Zagotta et al., 1989a, 1989b; Joho et al., 1990; Koren et al., 1990, Moorman et al., 1990).

Structural models of Na^+ and Ca^{2+} channels in which the channel is formed by four domains surrounding a central aqueous pore have been proposed (Greenblatt et al., 1985; Guy and Seetharamulu, 1986; Noda et al., 1986a; Catterall, 1988). Each domain consists of a core region of six (Noda et al., 1986a; Catterall, 1988) or more (Greenblatt et al., 1985; Guy and Seetharamulu, 1986) transmembrane α helices, flanked by cytoplasmic domains. The derived amino acid sequences of voltage-dependent K^+ channels are much shorter and correspond to one such domain (Figure 1). The largest degree of homology exists in the putative transmembrane regions, with a few charged residues in S2, S3, and S4 being strictly conserved among all voltage-dependent channels. The voltage sensor has been uniformly assigned to S4, and the channel pore has been variously assigned to S2 (Noda et al., 1984), S3 (Greenblatt et al., 1985; Oiki et al., 1988), or part of the conserved region between S5 and S6 (Guy and Seetharamulu, 1986). The effects of point mutations in S4 support its role in voltage sensing (Stühmer et al., 1989a; Auld et al., 1990).

The transmembrane segments are conserved, but the putative cytoplasmic amino (N) and carboxyl (C) termini show far more divergence, even among closely related channels. A growing body of evidence suggests a relationship between sequence variation in cytoplasmic termini and functional diversity. Splice variants of the *Shaker* K^+ channel from Drosophila (Kamb et al., 1988; Schwarz et al., 1988) differing in their N- and C-termini, yet sharing a common region that includes the first five transmembrane segments, have different kinetics of inactivation, when expressed in Xenopus oocytes (Iverson et al., 1988; Timpe et al., 1988b). Four rat brain K^+ channels encoded by the *rck* family (*rck1, 3, 4, and 5*) having virtually identical transmembrane segments (Stühmer et al., 1989b) show different kinetics of activation and inactivation. Some of the differences have been assigned to the short extracellular regions linking the transmembrane segments, although the channels also differ in their N- and C-termini.

To investigate directly how the putative cytoplasmic domains affect function, we made a series of deletions in the N- and C-termini of the delayed rectifier K^+ channel from rat brain encoded by the *drk1* gene (Frech et al., 1989). Among K^+ channels studied so far, only this channel has an unusually long C-terminus. We found the following: Deletions in either terminus affected both activation and inactivation; a small deletion at the N-terminus or a large deletion at the C-terminus resulted in a shift of the voltage dependence of activation and deactivation in the hyperpolarizing direction; larger deletions at the N-terminus removed inactivation and dramatically slowed activation and deactivation; and kinetics were largely restored in a truncated *drk1* channel that had most of both termini removed. It is therefore concluded, that the N- and C-termini are not essential for voltage-dependent activation, inactivation, and deactivation, although they can have profound modulatory effects on these parameters.

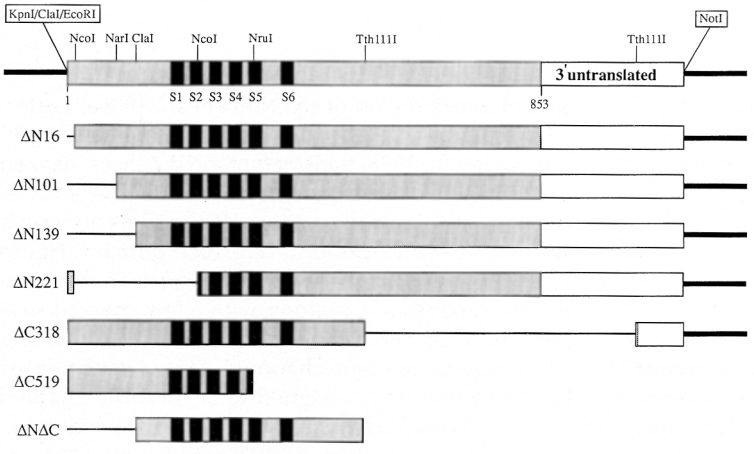

Figure 1. Restriction Sites and Deletion Mutants of *drk1*

A delayed rectifier K^+ channel cDNA clone from rat brain *drk1* is shown as an insert in the phagemid vector pBluescript SK[−]. Relative positions of restriction endonuclease sites used in this study are indicated; restriction sites in the polylinker region of pBluescript are boxed. The coding region is shaded, and the six putative transmembrane segments (S1–S6) that define the central core region are shown in black. The extent of the deletions is indicated by a fine line. The names of the deletion mutants are shown on the left. Note that mutant ΔN221 has S1 and part of S2 deleted, and mutant ΔC519 is missing S6 and part of S5. Clone ΔC318 codes for a protein of 540 amino acids. It is identical to the *drk1* protein up to the threonine at position 535, but lacks the C-terminal 318 amino acids of the *drk1* protein. Instead, ΔC318 contains at its C-terminus an additional 5 amino acids (Pro-Val-Gly-Val-Ser) derived from the 3′ untranslated region of *drk1*, followed by a stop codon.

Results

Expression of Functional K^+ Channels by Deletion Mutants

To investigate the functional role of cytoplasmic domains flanking the core region of the *drk1* channel, a series of mutants was generated in which progressively larger parts of the N- and C-termini were deleted (Figure 1). The N-terminus of the *drk1* protein is 182 amino acids long. The three N-terminal deletion mutants that left the central core region intact (ΔN16, ΔN101, and ΔN139) expressed functional K^+ channels. No voltage-dependent K^+ currents could be detected in oocytes expressing the N-terminal deletion mutant ΔN221, which had S1 and part of S2 removed (data not shown). The *drk1* protein has an unusually long C-terminus of 443 amino acids, constituting more than half of the protein (853 amino acids). Removal of the last 318 C-terminal amino acids of the protein encoded by *drk1* (ΔC318) still allowed formation of functional K^+ channels. However, removal of 519 C-terminal amino acids, including S6 and part of S5 (ΔC519), no longer produced voltage-sensitive K^+ current in Xenopus oocytes (data not shown). The double mutant ΔNΔC, a combination of ΔN139 and ΔC318, which lacks 139 amino acids of the N-terminus and 318 amino acids of the C-terminus, yielded functional K^+ channels.

A comparison of the K^+ currents expressed by *drk1* channels and the functional deletion mutants is shown in Figure 2. Both ΔN16 and ΔC318 expressed currents that activated slightly faster than the *drk1* current, when compared at the same membrane potential. ΔN101 and ΔN139 expressed channels having dramatically altered kinetics: activation was very slow, while inactivation was removed. The profound alterations in kinetics caused by deletion mutant ΔN139 alone were partially restored in the double mutant: activation was faster and inactivation was completely restored.

Voltage Dependence and Kinetics of Activation

Figure 3 compares families of currents for the *drk1*-encoded channel and its deletion mutants produced by a wide range of test potentials. All currents rose to a peak following, in most cases (vide infra), a sigmoidal time course, remained steady, and usually decreased at longer times. The functional deletion mutants fell into three groups (Figure 2A; Figure 3): ΔN16 and ΔC318 currents activated slightly faster than *drk1* current, ΔN101 and ΔN139 channels activated considerably slower and the threshold of activation was shifted to more positive potentials, and ΔNΔC channels had intermediate activation kinetics. To study the effect of the deletions on the voltage dependence of activation, the steady-state open probability was estimated. Since the instantaneous current–voltage relationships were nonlinear (Figure 4A), permeability rather than conductance was used as a measure of channel open probability. Permeability values were calculated from the currents at the end of 400 ms test pulses and were normalized to obtain steady-state activation curves. Assuming that the number of channels is not a function of membrane potential, normalized permeability curves measure the fraction of open channels as a function of voltage.

The steady-state activation curves for *drk1* channels and the deletion mutants were not well described by a single Boltzmann equation, which is to be expected when opening of the channels involves more than a first order gating step. However, it has been shown for multistep gating reactions at very negative potentials that the steepness of the voltage dependence is determined only by the total charge movement and not by the number and nature of the individual reaction steps (Almers, 1978). Therefore, the threshold region and the steeply rising part of the steady-state activation curves were fitted with the Boltzmann equation to obtain values for the slope parameter and midpoint potential of activation (Figure 4B; Table 1). The slope parameter thus obtained is similar to the limiting loga-

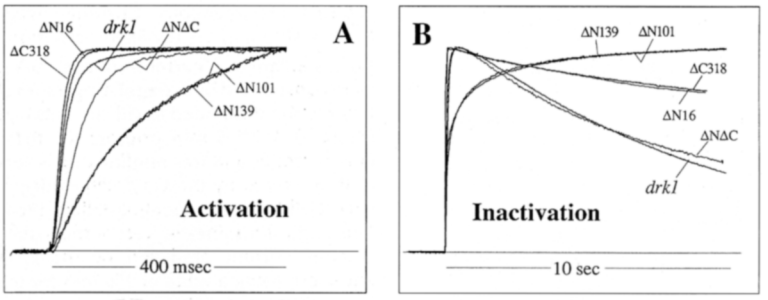

Figure 2. Deletion Mutants Express Channels with Modified Activation and Inactivation Kinetics

Xenopus oocytes were injected with runoff transcripts from *drk1* and the various deletion mutants, incubated for 3–4 days, defolliculated, and voltage-clamped. Holding potential was −80 mV. (A) Currents were elicited by a 400 ms test pulse to 0 mV (*drk1*, ΔN16, ΔC318, and ΔNΔC) or +20 mV (ΔN101 and ΔN139) and normalized to facilitate comparison. The slightly faster activation kinetics of ΔN16 and ΔC318 were significant and resulted from a shift of 5 mV in the hyperpolarizing direction of both steady-state activation and time constants of activation (Figure 5; Table 1). When corrected for this shift, activation kinetics were similar. Deletion mutants ΔN101 and ΔN139 have very slow activation kinetics, and their steady-state activation curve is shifted 20 mV in the depolarizing direction (Table 1). Currents are shown at +20 mV, for these two mutants, to illustrate the fact that the slow activation kinetics cannot be explained by this shift alone. Activation kinetics of the double mutant ΔNΔC, which is a combination of ΔN139 and ΔC318, are largely restored: ΔNΔC activates considerably faster than ΔN139, although still slower than *drk1* channels.

(B) Currents elicited by 10 s test pulses to 0 mV (*drk1*, ΔN16, ΔC318, and ΔNΔC) or +20 mV (ΔN101 and ΔN139). Like other delayed rectifiers, *drk1* channels displayed slow and incomplete inactivation. ΔN16 and ΔC318 inactivated less, whereas ΔN101 and ΔN139 continued to activate throughout the 10 s test pulse. Inactivation was completely restored in the double mutant ΔNΔC.

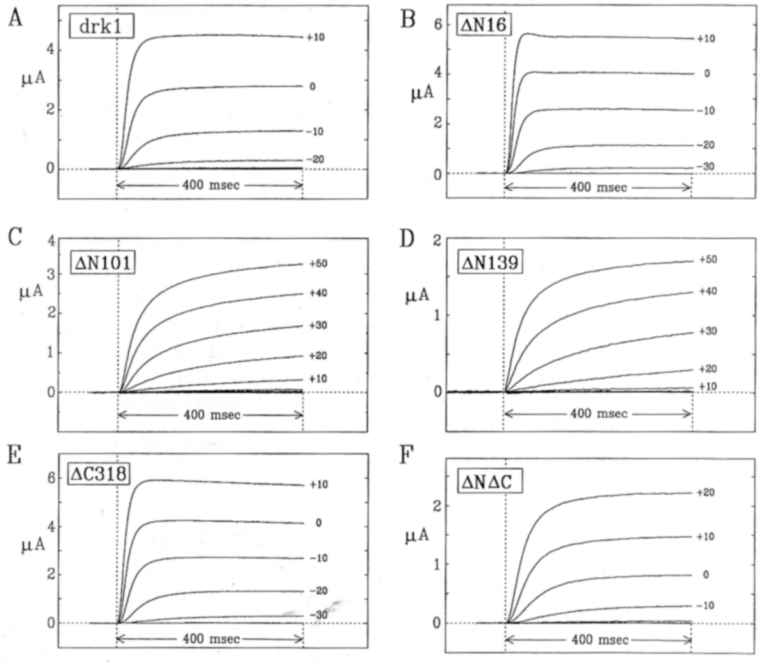

Figure 3. Families of Currents Expressed by *drk1* Channels and Deletion Mutants

Families of currents elicited by 400 ms test pulses to different voltages, indicated to the right of each current trace. Holding potential was −80 mV. Linear capacitive and leakage currents were removed by adding responses to small hyperpolarizing test pulses (P/4 method). Dotted lines indicate the beginning of the pulse.

rithmic potential sensitivity introduced by Almers (1978) and yields a lower limit for the total amount of (equivalent) gating charge involved in channel opening.

The steady-state activation curve for *drk1* channels had a midpoint potential of −9 mV and a slope parameter, k, of 6.6 mV, which corresponds to a minimum of 4 equivalent gating charges moving through the entire membrane field. The curves for deletion mutants ΔN16 and ΔC318 had midpoint potentials that were 5 mV more negative and similar slope parameters. As a result, the thresholds for activation were shifted to more hyperpolarizing potentials. The isochronal (400 ms) activation curves of ΔN101 and ΔN139 showed more dramatic shifts of 30 mV in the depolarizing direction, again without an effect on the slope parameter. Since activation of ΔN101 and ΔN139 was extremely slow (Figure 2B), steady state was reached only after 10 s. Normalized permeability curves for these two mutants were also obtained at 10 s. At steady state, the midpoint remained shifted 20 mV to more depolarized potentials, with no significant change in the slope parameter (Table 2).

The differences in kinetics are summarized in Figure 5. The widely used Hodgkin and Huxley (1952) model for activation of the delayed rectifier in squid axon was employed to describe quantitatively the activation kinetics of channels encoded by *drk1*, ΔN16, ΔC318, and ΔNΔC, since this model gave an accurate description of the sigmoidal time course (Figure 5A). No single value of the exponent that gave an acceptable description for all voltages could be found, and the exponent was optimized for each curve. Figure 5A

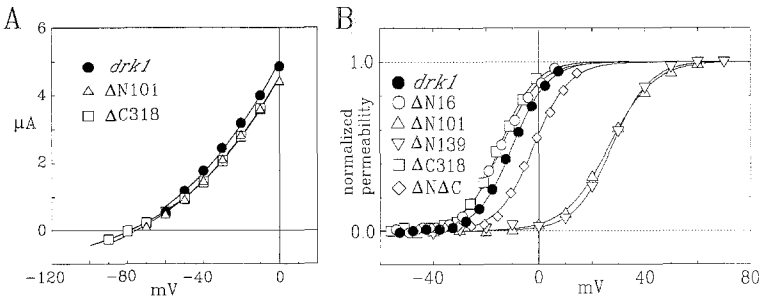

Figure 4. Instantaneous Current-Voltage Relationship and Steady-State Activation

(A) Instantaneous current-voltage curves were constructed by extrapolating a sum of two exponentials fitted to tail currents (see Figure 7). With 5 mM external K^+, these curves rectify, and this nonlinearity is very well described by the Goldman-Hodgkin-Katz (GHK) current equation (Hille, 1984). The continuous lines represent the instantaneous current predicted by the GHK equation, using a value of 100 mM for the internal K^+ concentration. Therefore, permeability rather than conductance was used to measure the steady-state open probability as a function of voltage.

(B) The current at the end of a test pulse is converted to a permeability using the GHK current equation, normalized, and plotted against the potential. The steady-state activation curve thus obtained is fitted with the Boltzmann equation shown as a continuous line. The form of the Boltzmann equation used is

$$P(E_m) = 1/[1 + \exp((E_{0.5} - E_m)/k)]$$

where k = 25/q mV, and q = equivalent gating charge. From this fit, a slope parameter (k) and the midpoint potential ($E_{0.5}$) are obtained. The steady-state activation curve of deletion mutants ΔN16 and ΔC318 shows a small (−5 mV) but significant shift in the hyperpolarizing direction. For deletion mutants ΔN101 and ΔN139, activation has not yet reached steady state at 400 ms. Their normalized permeability (isochronal activation) curves were shifted by +30 mV. Steady-state activation curves were obtained for these two mutants by using 10 s pulses. Activation curves were still shifted by +20 mV. The steady-state activation curve of the double mutant ΔNΔC, which combines ΔN139 and ΔC318, was shifted only by +9 mV.

Table 1. Steady-State Activation Parameters

	Duration (s)	$E_{0.5}$ (mV)	k (mV)	N
drk1	0.4	−9.2 ± 3.8	6.6 ± 1.0	6
ΔN16	0.4	−14.2 ± 4.4*	6.8 ± 1.3	16
ΔN101	0.4	+20.5 ± 5.2*	7.5 ± 1.4	4
ΔN101	10	+10.4 ± 4.0*	7.4 ± 0.6	4
ΔN139	0.4	+27.2 ± 1.4*	7.7 ± 1.4	5
ΔN139	10	+11.2 ± 4.4*	6.8 ± 1.0	4
ΔC318	0.4	−14.3 ± 5.6*	6.5 ± 1.0	11
ΔNΔC	0.4	−0.3 ± 3.8*	7.3 ± 0.7	8

Normalized permeability curves were fitted with the Boltzmann equation to obtain values for the slope parameter k and the midpoint potential $E_{0.5}$. For each parameter, the mean, standard deviation, and number of oocytes (N) are given. An asterisk indicates that the value differs significantly from *drk1* (Student's t-test, $P < 0.03$). Duration refers to the length of the test pulse.

Table 2. Steady-State Inactivation Parameters

	$E_{0.5}$ (mV)	k (mV)	Y_0	N
drk1	−19.0 ± 1.5	5.0 ± 0.9	0.25 ± 0.14	9
ΔN16	−18.8 ± 3.9	8.2 ± 1.9*	0.52 ± 0.16*	6
ΔC318	−18.3 ± 6.3	11.7 ± 5.5*	0.66 ± 0.08*	6
ΔNΔC	−17.3 ± 2.3	4.9 ± 0.3	0.28 ± 0.04	5

Prepulse inactivation curves were fitted with the Boltzmann equation (Figure 6) to obtain values for the slope parameter k, the midpoint potential $E_{0.5}$, and noninactivating fraction Y_0. The table lists the mean, standard deviation, and number of oocytes (N). An asterisk indicates that the value is significantly different from *drk1* (Student's t-test, $P < 0.03$).

shows examples of such curve fits for *drk1*, ΔN16, ΔC318, and ΔNΔC channels. The time constant of activation (τ_n) for *drk1* channels ranged from 8 to 100 ms (Figure 5B), and the exponent increased with depolarization from less than 2 (at threshold) to more than 4 at the most depolarized potentials (Figure 5C). Deletion mutants ΔN16 and ΔC318 had very similar activation kinetics, except that their curves were shifted in the hyperpolarizing direction. Activation kinetics of the double mutant ΔNΔC were shifted in the depolarizing direction, while the exponent depended less steeply on voltage.

The kinetics of mutants ΔN101 and ΔN139 were identical, yet significantly different from the the kinetics of *drk1* channels. Not only was activation extremely slow, it appeared to involve several time scales, and the sigmoidal character was almost completely lost. Therefore, the Hodgkin and Huxley model could not be used to describe the kinetics of these deletion mutants, and we were forced to use a more general model, a sum of exponentials. Three exponentials were necessary and sufficient (Figure 5D) to describe the activation kinetics. All three time constants of activation were considerably larger than the τ_n of the other constructs, even after correction for the shift of the steady-state activation curve. The fastest time constant (τ_1) ranged from 40 to 400 ms; the slowest (τ_3) ranged from 2 to 10 s (Figure 5E). The relative amplitudes of the three exponentials were converted to permeabilities and plotted against voltage (Figure 5F). All three relative permeabilities showed a similar voltage dependence: an initial steep increase with depolarization that gradually leveled off. The curves were shifted along the voltage axis with respect to each other, with the amplitude of the slowest time constant (*a3*) rising first and the fastest one (*a1*) rising last. As a result, at threshold the currents were dominated by the slow component, while at more depolarized potentials all three components contributed.

Voltage Dependence and Kinetics of Inactivation

Like other delayed rectifiers, *drk1* channels inactivated with a time constant of several seconds and part

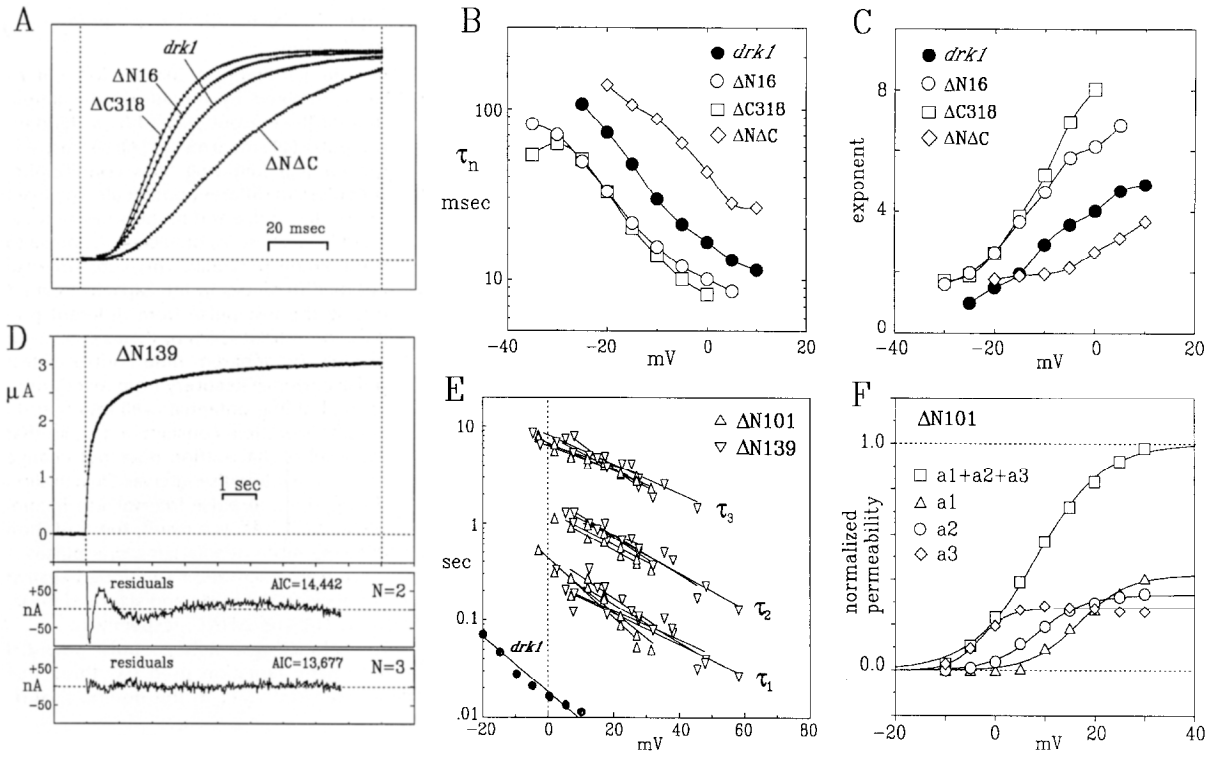

Figure 5. Effects of Deletions on Kinetics of Activation

(A–C) Activation kinetics of *drk1*, ΔN16, ΔC318, and ΔNΔC channels were sigmoidal. Current records were therefore fitted with the following equation (Hodgkin and Huxley, 1952):

$$I(t) = I \cdot [1 - \exp(-t/\tau_n)]^a$$

The adjustable parameters are I (the maximum current), τ_n (the time constant of activation), and the exponent *a*. It proved to be impossible to get acceptable fits for all voltages, using a single value for the exponent; therefore the parameter *a* was optimized for each curve. Parameter optimization was done by a nonlinear least squares routine, using the Marquardt-Levenberg algorithm. (A) shows examples of such fits at a test potential of 0 mV. The number of data points used for the fit was adjusted so that the current had reached at least 95% of its maximum. Only the first 100 ms of the fits are shown to illustrate the difference in kinetics better. Time constants of activation as a function of voltage are shown in (B); the exponent *a* as a function of voltage is shown in (C). Deletion mutants ΔN16 and ΔC318 have faster kinetics than *drk1* channels, which appears to result from a 5 mV shift of the τ-voltage curve in the hyperpolarizing direction. The double mutant ΔNΔC activated slower than *drk1* channels, and its τ-voltage curve appears shifted in the depolarizing direction. In all cases the exponent increases with voltage. The curves for ΔN16 and ΔC318 again appear to be shifted in the hyperpolarizing direction. The curve for ΔNΔC appears shifted in the depolarizing direction, but is also less steeply voltage-dependent. (D–F) Activation kinetics of ΔN101 and ΔN139 were not sigmoidal and considerably slower. A sum of exponentials was chosen as a model for the activation kinetics of these mutations:

$$I(t) = A + \sum_{i=1}^{N} a_i \cdot \exp[-t/\tau_i]$$

Current records were fitted with one, two, three, and four exponentials using a nonlinear least squares (Marquardt-Levenberg) routine. The asymptotic information criterium or AIC, adapted for least squares problems (DiStefano and Landaw, 1984), was used to discriminate among models:

$$AIC = N \cdot \log(RSS) + 2P$$

where N = number of data points; RSS = residual sum of squares; P = number of parameters. The number of exponentials that minimized AIC was considered the best model. (D) illustrates the procedure by showing a sum of three exponentials (continuous line) superimposed on a current record. The lower panels show the residuals for sums of two or three exponentials, respectively. Note the oscillations in the residuals for the sum of two exponentials. Four exponentials did not improve the fit significantly (as measured by AIC). For all current records analyzed in this way, a sum of three exponentials yielded a minimum AIC. (E) summarizes the results by showing the three time constants as a function of voltage. The solid straight lines were obtained by linear least squares fits to each curve. The time constants of activation for *drk1* channels are shown as solid circles for comparison. (F) illustrates how the relative amplitudes of the three exponentials depended on voltage. The relative amplitudes were converted to permeabilities (see Figure 4), and their sum was normalized.

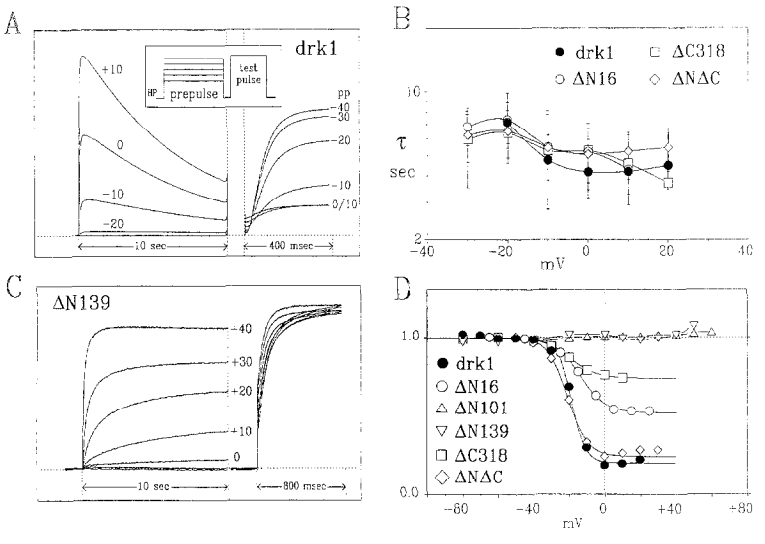

Figure 6. Effects of Deletions on Prepulse Inactivation

(A and C) Prepulse inactivation curves were obtained by measuring the amplitude of the current elicited by a standard test pulse (400 ms, 0 mV for [A]; 800 ms, +50 mV for [C]) following 10 s conditioning prepulses to different potentials (see inset of [A]). Test pulse and prepulse were separated by a 50 ms (A) or 100 ms (C) pulse to the holding potential. This short interval avoids differences in the capacity current during the test pulse from different prepulse potentials, which by themselves might change the apparent time course of test pulse currents. Recovery from inactivation at the holding potential (−80 mV) is sufficiently slow (time constant = 1 s), so that the level of inactivation does not change during the interpulse interval. Deactivation during the interpulse interval was incomplete in (C), and as a result, the activation kinetics during the test pulse depended on the prepulse: activation kinetics were faster following more depolarizing pre- pulses.

(B) The time course of inactivation was very well fitted by a single exponential. The time constants of inactivation are plotted against voltage. Because there was a relatively large variability in the these time constants for different oocytes, the mean and standard deviations are given. The number of oocytes used in each case was 8, 6, 8, and 5 for *drk1*, ΔN16, ΔC318, and ΔNΔC, respectively.

(D) The amplitudes of the steady-state currents elicited by the test potentials were normalized and plotted against the prepulse potential (symbols) and fitted with the Boltzmann equation (continuous line). The form of the Boltzmann equation used has three free parameters: $E_{0.5}$ (the midpoint potential), k (slope parameter), and Y_0, the right asymptote, corresponding to the noninactivating fraction:

$$Y(E_m) = Y_0 + [1 - Y_0]/[1 + \exp((E_{0.5} - E_m)/k)]$$

of the current was resistant to inactivation (Schwarz and Vogel, 1971; Chabala, 1984; Gundersen et al., 1984; Clay, 1990). Prepulse inactivation curves were measured for *drk1* channels and all the functional deletion mutants using a standard two-pulse protocol and fitted with the Boltzmann equation (Figure 6D; Table 2). The midpoint potential for inactivation of *drk1* channel was −19 mV, the slope parameter, k, was 5 mV, and 25% of the current was resistant to inactivation. Inactivation for deletion mutants ΔN16 and ΔC318 was less complete (noninactivating components were 52% and 66% respectively) and less steeply voltage-dependent (k = 8 and k = 12 mV, respectively), but there was no effect on the midpoint potential. Deletion mutants ΔN101 and ΔN139 showed no inactivation on this time scale (Figures 6C and 6D). For the double mutant ΔNΔC, inactivation was restored, with a midpoint potential, slope parameter, and noninactivating fraction not significantly different from those of *drk1* channels.

The time course of inactivation could be well fitted with a single exponential. Time constants of inactivation showed very little voltage dependence (Figure 6B), being slightly larger at threshold. Because of the shallow voltage dependence and the rather large variability, shifts in the voltage dependence of the time constants could not be determined.

Kinetics of Deactivation

Deactivation kinetics were studied using tail currents (Figure 7). In all cases, two exponentials were necessary and sufficient to describe deactivation. Time constants of deactivation for *drk1* channels were voltage-dependent (Figure 7C). Deactivation time constants for *drk1* and ΔN16 and ΔC318 channels had a very similar voltage dependence. Measured at the same time scale, deactivation was virtually absent for deletion mutants ΔN101 and ΔN139 (inset Figure 7B). Using 10 s tail currents, deactivation became apparent (Figure 7B), and again two time constants were needed for an accurate description. Their voltage dependence is shown in Figure 7C. Deactivation kinetics of the double mutant ΔNΔC were almost as fast as those for *drk1* channels, the difference being larger at more depolarized potentials (Figure 7C). The relative amplitudes of the two time constants of deactivation were very voltage-dependent for all channels, the fast time constant dominating at hyperpolarized potentials and the slow time constant being more important at depolarized potentials (Figure 7D).

Discussion

We have investigated the functional importance of the N- and C-terminal domains of a delayed rectifier K^+ channel from rat brain encoded by the *drk1* gene. The cDNA sequence of *drk1* predicts a protein of 853 amino acids. The proposed tertiary structure contains a central core region of six putative transmembrane segments (S1–S6) flanked by the N- and C-termini, which are thought to be cytoplasmic. Compared with other K^+ channels, the C-terminus of *drk1* protein is

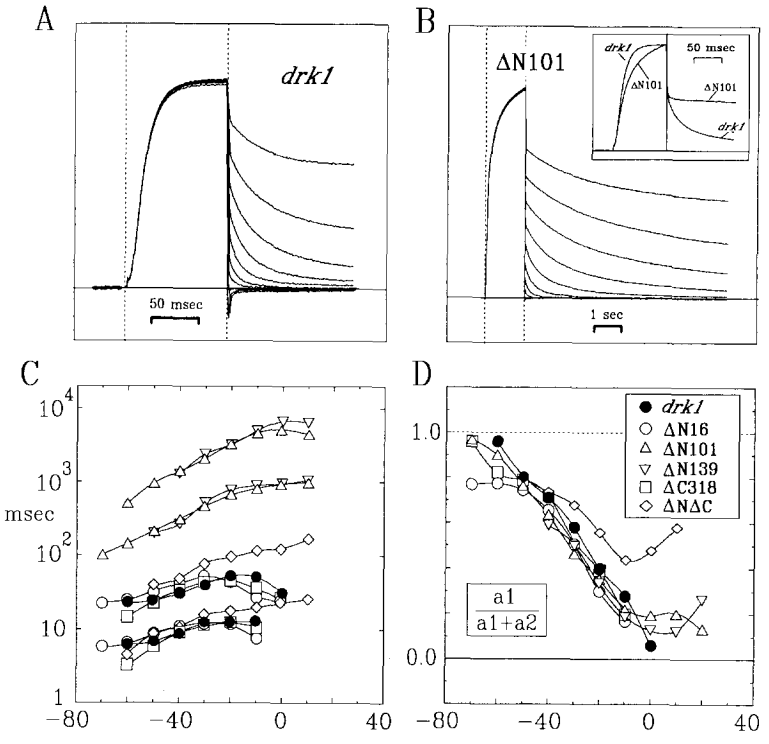

Figure 7. Effects of Deletions on Kinetics of Deactivation

Deactivation kinetics were studied by measuring tail currents. The pulse protocol consisted of a standard depolarizing prepulse (+10 mV, 100 ms for *drk1*, ΔN16, and ΔC318 channels; +40 mV, 2 s for ΔN101 and ΔN139 channels) followed by hyperpolarizing test pulses to different potentials. For all tail currents analyzed, a sum of 2 exponentials was necessary and sufficient. Examples of tail current measurements are given for *drk1* (A) and ΔN101 (B) channels. (C) shows the voltage dependence of both time constants of deactivation for *drk1* and the deletion mutant channels. The upper set of symbols refers to the slow component of deactivation; the lower, to the rapid component. Deletion mutants ΔN101 and ΔN139 have extremely slow deactivation kinetics. At a time scale where the *drk1* channel completely deactivates, there is almost no sign of deactivation for ΔN101 and ΔN139 channels (see inset of [B]). The relative amplitudes (*a1* and *a2*) of the fast and slow components of deactivation were steeply voltage-dependent, with the fast time constant dominating at hyperpolarized potentials and the slow one dominating at depolarized potentials (D).

relatively long (443 amino acids) and the N-terminus is relatively short (182 amino acids). By analogy with voltage-gated Na^+ and Ca^{2+} channels, it has been suggested that four subunits assemble to form a functional K^+ channel. The effects of deletions in the N- and C-terminus on macroscopic current kinetics were studied following expression of channels in Xenopus oocytes. Since for three out of four N-terminal deletions the original initiating methionine had been removed, the question arose as to where initiation occurs.

Translational Initiation Sites

In accordance with the "scanning model" of eukaryotic translation initiation (Kozak, 1989), we assume that protein synthesis initiates at the most upstream AUG. In the case of *drk1* and the deletion mutants, this assumption is reasonable, since the sequences flanking in frame AUG codons (Table 3) have all been observed at functional initiation sites in vertebrate mRNAs (Kozak, 1987). As shown in Figure 2, *drk1*, ΔN16, and ΔN101 had distinct functional characteristics and therefore should not initiate at the same site. We have established, through site-directed mutagenesis, that *drk1* initiates at AUG codon 1 and not at the second methionine (Met^{17}). Substituting Met^{17} for leucine, valine, or alanine had no effects on the functional characteristics of *drk1* protein (G. C. Frech, unpublished data). Taken together, these results are consistent with our assignment of initiation sites. Table 3 also lists the amount of RNA necessary to obtain several microamperes of K^+ current 3 days after injection. There is no clear correlation between frequency of occurrence of a particular initiation sequence and efficiency of functional expression in the oocyte. This is not surprising, since the level of expression is deter-

Table 3. Translation Initiation Sequences

	Initiation Sequence	Occurrence (%)	RNA Injected (ng per Oocyte)
drk1	**G G C** A T G **A**	6.7	0.1
ΔN16	**G G C** A T G **G**	18.6	2.0
ΔN101	**C A G** A T G **A**	0.3	10.0
ΔN139	**C A G** A T G **A**	0.3	10.0
ΔN221	**G G C** A T G **A**	6.7	15.0*
ΔC318	**G G C** A T G **A**	6.7	10.0
ΔC519	**G G C** A T G **A**	6.7	15.0*
ΔNΔC	**C A G** A T G **A**	0.3	10.0

Nucleotide sequences surrounding the most upstream in frame ATG codon (underlined) are shown for *drk1* and the deletion mutants. The bases at position −3 and +4, which are most important for efficient translation initiation, are shown in boldface. The frequency of occurrence as an initiation sequence in 699 vertebrate mRNAs (Kozak, 1987) is listed. The amount of RNA necessary to obtain 3–10 μA of outward current (at +40 mV) 3 days after injection is given. An asterisk indicates that no expressed K^+ current could be detected (N = 7 for ΔN221 and N = 5 for ΔC519, in 3 batches of oocytes that expressed *drk1*).

Analysis of hundreds of vertebrate mRNA sequences has revealed that the first AUG serves as the site for translation initiation, as long as it lies in a favorable context (Kozak, 1986, 1987). Mutant ΔN139 contains an out of frame ATG (nucleotide positions 362–364 in the *drk1* sequence) upstream of the proposed initiation triplet (Met^{140}). This creates a short open reading frame ending at TGA 419–421, right after Met^{140}. The 5′ proximal ATG triplet is flanked by a T at position −3 and by an A at position +4, a configuration never observed at functional vertebrate initiator codons (Kozak, 1987).

mined by many factors, including translation initiation efficiency, protein stability, membrane insertion, and subunit assembly.

Effects of Deletions on Function

All deletion mutants that left the central core region of six putative transmembrane segments (S1–S6) intact yielded functional K^+ channels when expressed in Xenopus oocytes. Two deletions that removed either the N-terminus including S1 (ΔN221), or the C-terminus including S6 (ΔC519) did not yield detectable K^+ currents in Xenopus oocytes. These results are consistent with the proposed topography and underline the functional importance of all transmembrane segments. Removing 16 amino acids from the N-terminus (ΔN16) or 318 amino acids from the C-terminus (ΔC318) had only minor effects on kinetics. However, two deletion mutants missing 101 and 139 amino acids from the N-terminus (ΔN101 and ΔN139) had dramatically altered kinetics (Figure 2): activation kinetics were slowed considerably, steady-state activation curves were shifted 20–30 mV in the depolarizing direction, and inactivation was removed. When 318 amino acids were removed from the C-terminus of ΔN139 to obtain the double mutant ΔNΔC, most of the changes produced by ΔN139 were reversed: inactivation was completely restored, steady-state activation was shifted toward control, and activation and deactivation kinetics were partially restored.

Structural Implications

The present results have several implications for the relation between structure and function of voltage-dependent K^+ channels. Changes in either the N- or the C-terminus affected both activation and inactivation. Activation can become faster or considerably slower. The more subtle changes shown by ΔN16 and ΔC318 can be explained by a shift of both steady-state activation and time constants of activation in the hyperpolarizing direction, without an effect on the steepness of their voltage dependence. A simple interpretation of these results is to assume the existence of a charged region in both the N- and C-termini that is close enough to the voltage sensor (S4) to distort the electric field locally, in the same way as a fixed surface charge. Assuming that both termini are cytoplasmic, a shift in the hyperpolarizing direction caused by ΔN16 and ΔC318 implies the removal of negative charge. Only 1 of the first 16 N-terminal residues is negatively charged (Glu^{14}), whereas the last 318 residues of the C-terminus contain 34 negatively charged residues and 30 positive ones, giving a net charge of −4 for this segment. However, deletion of 101 or 139 residues from the N-terminus produces disparate changes in the both the rate and mechanism of activation that cannot be explained by a simple distortion of the field perceived by the voltage sensor. The shift in voltage dependence of activation in the depolarizing direction without a change in slope, is consistent with the removal of a positively charged domain and/or the appearance of a negatively charged structure at the cytoplasmic face of the protein, in close proximity of S4. But the changes in kinetics of activation cannot be explained by a simple shift of the voltage dependence. This suggests that the (outward) movement of S4 may be more directly retarded. A large enough change in negative charge might have such an effect through electrostatic interaction with S4. Alternatively, these deletions could result in a conformational change that mechanically hinders, but does not prevent movement of S4.

Concomitant with the slowing of activation kinetics, inactivation is apparently absent for mutants ΔN101 and ΔN139. Since inactivation is incomplete for *drk1*, channels are still able to open in this "inactivated" state, and the probability of opening depends on voltage (Figure 6). Therefore, incompletely inactivated channels would still show voltage-dependent activation and deactivation, although the rates would be slowed. For example, the rate of activation produced by the same test pulse is slower for prepulses to −40 mV than for those to +10 mV (Figure 6A). One interpretation of the apparent lack of inactivation is therefore that the channels expressed by ΔN101 and ΔN139 behave like *drk1* channels which have been inactivated. Contrary to *drk1* channels, inactivation for ΔN101 and ΔN139 channels cannot be removed by hyperpolarization. The interpretation that ΔN101 and ΔN139 produce permanently, though incompletely inactivated *drk1* channels suggests that the slow activation kinetics of these two mutants is not a novel property, but rather reflects a behavior inherent to *drk1* channels that is normally masked by inactivation.

Most of the functional changes introduced by deleting 139 residues of the N-terminus can be reversed by deleting an additional 318 residues from the C-terminus (Figure 2, ΔNΔC). These results suggest that the C-terminal domain is directly responsible for the functional changes caused by the N-terminal deletions ΔN101 and ΔN139. This means that the two domains interact, so that a deletion in the N-terminal domain allows the C-terminus to interfere with activation, i.e., by presentation of negative charges in the proximity of S4. Such an interaction implies that the two domains are located on the same side of the membrane, consistent with the proposed transmembrane arrangement.

The double mutant ΔNΔC approaches a "minimal channel," from which large parts of both the N- and C-termini have been deleted, while retaining most of the functional characteristics of the parent delayed rectifier K^+ channel. The channel formed by double mutant ΔNΔC consists of 396 amino acids, which is smaller than any of the published functional K^+ channels. Additional experiments are planned to define more precisely the minimal sequence required to preserve function.

The restoration of inactivation in the double mutant ΔNΔC does not support an interpretation in terms of the ball and chain model proposed for the fast inacti-

vation of the Na^+ channel (Armstrong and Bezanilla, 1977) and the *Shaker* K^+ channel (Hoshi et al., 1989, Soc. Neurosci., abstract). In this model, a positively charged cytoplasmic domain (ball), connected to the rest of the protein by a chain, swings into the internal mouth of the open pore during prolonged depolarization to inactivate the channel. Removal of inactivation by deletion of 101 or 139 residues from the N-terminus is consistent with a positively charged domain of the N-terminus being the "ball," but the restoration of inactivation in the double mutant challenges such an interpretation. Since the delayed rectifier inactivates much slower than the Na^+ channels or A-type K^+ channels, our results do not exclude the "ball and chain" model as a possible mechanism for fast inactivation.

Although there were dramatic effects on activation and inactivation, it is remarkable that none of the deletions affected the slope of the steady-state activation curve (Figure 4B; Table 1). This is consistent with the idea that this slope is determined by the number of gating charges (in S4) moving across the membrane in response to a depolarization, causing a conformational change allowing the channels to open.

In conclusion, the results presented here show that the N- and C-terminal domains can alter kinetics of both activation and inactivation, shift the voltage dependence of activation, without affecting the steepness, interact with each other (and therefore may be on the same side of the membrane), and are not necessary for voltage-dependent activation or inactivation. We propose, therefore, that one of the functional roles of the cytoplasmic domains is to modulate activation and inactivation. They are not essential, however, since a truncated version of the *drk1* protein, which is missing most of both termini, has all the properties of a delayed rectifier K^+ channel.

Experimental Procedures

Standard Recombinant DNA Techniques

Standard methods of plasmid DNA preparation, restriction enzyme analysis, agarose gel electrophoresis, DNA-modifying enzymatic reactions, and bacterial transformation were used (Maniatis et al., 1982; Berger and Kimmel, 1987). The parent clone *drk1* (Frech et al., 1989) as well as the *drk1*-derived truncated mutants were propagated in the transcription-competent phagemid vector pBluescript SK[−] (Stratagene).

Construction of Truncated Mutants of *drk1*

N- and C-terminal deletion mutants were constructed using the restriction endonuclease sites shown in Figure 1.

N-Terminal Deletion Mutants

To obtain the deletion mutant ΔN16, *drk1* was first digested to completion with KpnI, which cleaves in the polylinker of pBluescript at nucleotide position −66, and then partially digested with NcoI (+47 and +710). After filling in the ends with T4 DNA polymerase in the presence of deoxynucleoside triphosphates, the 6.3 kb restriction fragment was isolated by agarose gel electrophoresis. Deletion mutant ΔN101 was created by digesting *drk1* with EcoRI (−22) and with NarI (+257). After treating with T4 DNA polymerase to obtain flushed ends, the 6.1 kb restriction fragment was isolated. To obtain the deletion mutant ΔN139, *drk1* was digested with ClaI (−39 and +359), and for the deletion mutant ΔN221, *drk1* was digested with NcoI (+47 and +710). All isolated fragments were purified with "Geneclean" (Bio 101, Inc.), recircularized using T4 DNA ligase, and then used to transform E. coli strain XL1-Blue. The nucleotide sequences at the 5′ ends of all N-terminal deletion mutants were confirmed by restriction enzyme analysis and by DNA sequence analysis.

C-Terminal Deletion Mutants

Deletion mutant ΔC318 was constructed by digesting *drk1* with Tth111I (+1605 and +3089). After filling in the ends with T4 DNA polymerase, the long restriction fragment (4.9 kb) was isolated by agarose gel electrophoresis, ligated, and used to transform E. coli strain XL1-Blue. The nucleotide sequence at the 3′ end of the coding region of ΔC318 was determined. Deletion mutant ΔC519 was obtained by linearizing *drk1* with NruI (+1003) and using the template for runoff transcription. The double mutant ΔNΔC is a combination of ΔN139 and ΔC318, which was obtained by linearizing ΔN139 with Tth111I (+1605).

In Vitro Transcription and Oocyte Injection

Preparation of cRNA and oocyte injection has been described previously (Joho et al., 1990). Stage V or VI oocytes were injected with 75 nl of cRNA solutions and tested for the expression of functional K^+ channels 3 or 4 days after injection. Before electrophysiological recordings were performed, the follicular layer of cells was removed manually from the oocytes.

Electrophysiology

Oocytes were voltage-clamped using a commercial two-electrode voltage-clamp amplifier (Axoclamp 2A, Axon Instruments). Glass electrodes were filled with 3 M KCl, 10 mM HEPES (pH 7.40). The bath solution contained 100 mM NaMES (methanesulphonate), 5 mM KMES, 2 mM $MgCl_2$, 10 mM HEPES (pH 7.40 with Tris-base). Most Cl^- has been substituted with MES to shift the Cl^- reversal potential to a more positive potential. Together with the absence of Ca^{2+}, this helps to reduce the outward current in uninjected oocytes. This solution was perfused continuously at a rate of 2 ml/min. Under these conditions, uninjected oocytes or oocytes injected with 0.1 M KCl have less than 200 nA of outward current at maximal depolarizations, which at all potentials tested was less than 5% of the expressed K^+ currents in this study. All experiments were done at room temperature (22°C ± 1°C). The resistance of the current-carrying electrode in the bath varied between 1.0 and 2.0 MΩ; the resistance of the voltage-sensing electrode varied between 3 and 6 MΩ. For this configuration, the voltage-settling time (the time it takes to reach 95% of the voltage step) was 2 ms. The PClamp system (Axon Instruments) was used for the generation of voltage pulse protocols and data acquisition. Linear leakage and capacity currents were corrected on line using the P/4 method.

Acknowledgments

We wish to thank Gabriele Schuster for expert injection and handling of oocytes. This work was supported by the following grants: Advanced Technology Program Grant from the State of Texas to R. H. J; NS08805 to J. D.; NS23877 and HL37044 to A. M. B.

The costs of publication of this article were defrayed in part by the payment of page charges. This article must therefore be hereby marked "*advertisement*" in accordance with 18 U.S.C. Section 1734 solely to indicate this fact.

Received April 20, 1990; revised July 23, 1990.

References

Almers, W. (1978). Gating currents and charge movements in excitable membranes. Rev. Physiol. Biochem. Pharmacol. *82*, 96–190.

Armstrong, C. M., and Bezanilla, F. (1977). Inactivation of the sodium channel. II. Gating current experiments. J. Gen. Physiol. *30*, 567–590.

Auld, V. J., Goldin, A. L., Krafte, D. S., Marshall, J., Dunn, J. M., Catterall, W. A., Lester, H. A., Davidson, N., and Dunn, R. J.

(1988). A rat brain Na^+ channel α subunit with novel gating properties. Neuron *1*, 449–461.

Auld, V. J., Goldin, A. L., Krafte, D. S., Catterall, W. A., Lester, H. A., Davidson, N., and Dunn, R. J. (1990). A neutral amino acid change in segment IIS4 dramatically alters gating properties of the voltage-dependent sodium channel. Proc. Natl. Acad. Sci. USA *87*, 323–327.

Baumann, A., Krah-Jentgens, I., Müller, R., Müller-Holtkamp, F., Seidel, R., Kecskemethy, N., Casal, J., Ferrus, A., and Pongs, O. (1987). Molecular organization of the maternal effect region of the *Shaker* complex of *Drosophila*: characterization of an I_a channel transcript with homology to vertebrate Na^+ channel. EMBO J. *6*, 3419–3429.

Baumann, A., Grupe, A., Ackermann, A., and Pongs, O. (1988). Structure of the voltage-dependent potassium channel is highly conserved from *Drosophila* to vertebrate central nervous system. EMBO J. *7*, 2457–2463.

Berger, S. L., and Kimmel, A. R. (1987). Methods in Enzymology, Vol. 152, Guide to Molecular Cloning Techniques (New York: Academic Press, Inc.).

Butler, A., Wei, A., Baker, K., and Salkoff, L. (1989). A family of putative potassium channel genes in *Drosophila*. Science *243*, 943–947.

Catterall, W. A. (1988). Structure and function of voltage-sensitive ion channels. Science *242*, 50–61.

Chabala, L. D. (1984). The kinetics of recovery and development of potassium channel inactivation in perfused squid (*Loligo pealei*) giant axons. J. Physiol. *356*, 192–220.

Christie, M. J., Adelman, J. P., Douglass, J., and North, R. A. (1989). Expression of a cloned rat brain potassium channel in *Xenopus* oocytes. Science *244*, 221–224.

Clay, J. R. (1990). Slow inactivation and reactivation of the K channel in squid axons. A tail current analysis. Biophys. J. *55*, 407–414.

DiStefano, J. J., III, and Landaw, E. M. (1984). Multiexponential, multicompartmental, and noncompartmental modeling. II. Data analysis and statistical considerations. Am. J. Physiol. *246*, R665–667.

Frech, G. C., VanDongen, A. M. J., Schuster, G., Brown, A. M., and Joho, R. H. (1989). A novel potassium channel with delayed rectifier properties isolated from rat brain by expression cloning. Nature *340*, 642–645.

Greenblatt, R. E., Blatt, Y., and Montal, M. (1985). The structure of the voltage-sensitive sodium channel. Inferences derived from computer-aided analysis of the Electrophorus electricus channel primary structure. FEBS Lett. *193*, 125–134.

Gundersen, C. B., Miledi, R., and Parker, I. (1984). Slowly inactivating potassium channels induced in Xenopus oocytes by messenger ribonucleic acid from Torpedo brain. J. Physiol. 353, *231*–248.

Guy, H. R., and Seetharamulu, P. (1986). Molecular model of the action potential sodium channel. Proc. Natl. Acad. Sci. USA 83, 508–512.

Hille, B. (1984). Ionic Channels of Excitable Membranes (Sunderland, Massachusetts: Sinauer Associates Inc.).

Hodgkin, A. L., and Huxley, A. F. (1952). A quantitative description of membrane current and its application to conduction and excitation in nerve. J. Physiol. *117*, 500–544.

Iverson, L. E., Tanouye, M. A., Lester, H. A., Davidson, N., and Rudy, B. (1988). A-type potassium channels expressed from *Shaker* locus cDNA. Proc. Natl. Acad. Sci. USA *85*, 5723–5727.

Joho, R. H., Moorman, J. R., VanDongen, A. M. J., Kirsch, G. E., Silberberg, H., Schuster, G., and Brown, A. M. (1990). Toxin and kinetic profile of rat brain type III sodium channels expressed in *Xenopus* oocytes. Mol. Brain Res. *7*, 105–113.

Kamb, A., Iverson, L. E., and Tanouye, M. A. (1987). Molecular characterization of *Shaker*, a *Drosophila* gene that encodes a potassium channel. Cell *50*, 405–413.

Kamb, A., Tseng-Crank, J., and Tanouye, M. A. (1988). Multiple products of the *Drosophila Shaker* gene may contribute to potassium channel diversity. Neuron *1*, 421–430.

Kayano, T., Noda, M., Flockerzi, V., Takahashi, H., and Numa, S. (1988). Primary structure of rat brain sodium channel III deduced from the cDNA sequence. FEBS Lett. *228*, 187–194.

Koren, G., Liman, E. R., Logothetis, D. E., Nadal-Ginard, R., and Hess, P. (1990). Gating mechanisms of a cloned potassium channel expressed in frog oocytes and mammalian cells. Neuron *4*, 39–51.

Kozak, M. (1986). Point mutations define a sequence flanking the AUG initiator codon that modulates translation by eukaryotic ribosomes. Cell *44*, 283–292.

Kozak, M. (1987). An analysis of 5'-noncoding sequences from 699 vertebrate messenger RNAs. Nuc. Acids Res. *15*, 8125–8132.

Kozak, M. (1989). The scanning model for translation: an update. J. Cell Biol. *108*, 229–241.

Leonard, R. J., Karschin, A., Jayashree-Aiyar, S., Davidson, N., Tanouye, M. A., Thomas, L., Thomas, G., and Lester, H. A. (1989). Expression of *Drosophila Shaker* potassium channels in mammalian cells infected with recombinant vaccinia virus. Proc. Natl. Acad. Sci. USA *86*, 7629–7633.

Maniatis, T., Fritsch, E. F., and Sambrook, J. (1982). Molecular Cloning: A Laboratory Manual (Cold Spring Harbor, New York: Cold Spring Harbor Laboratory).

McKinnon, D. (1989). Isolation of a cDNA clone coding for a putative second potassium channel indicates the existence of a gene family. J. Biol. Chem. *264*, 8230–8236.

Mikami, A., Imoto, K., Tanabe, T., Niidome, T., Mori, Y., Takeshima, H., Narumiya, S., and Numa, S. (1989). Primary structure and functional expression of the cardiac dihydropyridine-sensitive calcium channel. Nature *340*, 230–233.

Moorman, J. R., Kirsch, G. E., VanDongen, A. M. J., Joho, R. H., and Brown, A. M. (1990). Fast and slow gating of sodium channels encoded by a single mRNA. Neuron *4*, 243–252.

Noda, M., Shimizu, S., Tanabe, T., Takai, T., Kayano, T., Ikeda, T., Takahashi, H., Nakayama, H., Kanaoka, Y., Minamino, N., Kangawa, K., Matsuo, H., Raftery, M. A., Hirose, T., Inayama, S., Hayashida, H., Miyata, T., and Numa, S. (1984). Primary structure of Electrophorus electricus sodium channel deduced from cDNA sequence. Nature *312*, 121–127.

Noda, M., Ikeda, T., Kayano, T., Suzuki, H., Takeshima, H., Kurasaki, M., Takahashi, H., and Numa, S. (1986a). Existence of distinct sodium channel messenger RNAs in rat brain. Nature *320*, 188–192.

Noda, M., Ikeda, T., Suzuki, H., Takeshima, H., Takahashi, T., Kuno, M., and Numa, S. (1986b). Expression of functional sodium channels from cloned cDNA. Nature *322*, 826–828.

Oiki, S., Danho, W., and Montal, M. (1988). Channel protein engineering: synthetic 22-mer peptide from the primary structure of the voltage-sensitive sodium channel forms ionic channels in lipid bilayers. Proc. Natl. Acad. Sci. USA *85*, 2393–2397.

Papazian, D. M., Schwarz, T. L., Tempel, B. L., Jan, Y. N., and Jan, L. Y. (1987). Cloning of genomic and complementary DNA from *Shaker*, a putative potassium channel gene from *Drosophila*. Science *237*, 749–753.

Salkoff, L., Butler, A., Wei, A., Scavarda, N., Giffen, K., Ifune, C., Goodman, R., and Mandel, G. (1987). Genomic organization and deduced amino acid sequence of a putative sodium channel gene in *Drosophila*. Science *237*, 744–749.

Schwarz, J. R., and Vogel, W. (1971). Potassium inactivation in single myelinated nerve fibres of *Xenopus laevis*. Pflügers Arch. *330*, 61–73.

Schwarz, T. L., Tempel, B. L., Papazian, D. M., Jan, Y. N., and Jan, L. Y. (1988). Multiple potassium-channel components are produced by alternative splicing at the *Shaker* locus in *Drosophila*. Nature *331*, 137–142.

Stühmer, W., Methfessel, C., Sakmann, B., Noda, M., and Numa, S. (1987). Patch clamp characterization of sodium channels expressed from rat brain cDNA. Eur. Biophys. J. *14*, 131–138.

Stühmer, W., Conti, F., Suzuki, H., Wang, X., Noda, M., Yahagi, N., Kubo, H., and Numa, S. (1989a). Structural parts involved in activation and inactivation of the sodium channel. Nature *339*, 597–603.

Stühmer, W., Ruppersberg, J. P., Schröter, K. H., Sakmann, B., Stocker, M., Giese, K. P., Perschke, A., Baumann, A., and Pongs, O. (1989b). Molecular basis of functional diversity of voltage-gated potassium channels in mammalian brain. EMBO J. *8*, 3235–3244.

Tanabe, T., Takeshima, H., Mikami, A., Flockerzi, V., Takahashi, H., Kangawa, K., Kojima, M., Matsuo, H., Hirose, T,. and Numa, S. (1987). Primary structure of the receptor for calcium channel blockers from skeletal muscle. Nature *328*, 313–318.

Tempel, B. L., Papazian, D. M., Schwarz, T. L., Jan, Y. N., and Jan, L. Y. (1987). Sequence of a probable potassium channel component encoded at the *Shaker* locus of *Drosophila*. *Science 237*, 770–775.

Tempel, B. L., Jan, Y. N., and Jan, L. Y. (1988). Cloning of a probable potassium channel gene from mouse brain. Nature *332*, 837–839.

Timpe, L. C., Jan, Y. N., and Jan, L. Y. (1988a). Four cDNA clones from the *Shaker* locus of Drosophila induce kinetically distinct A-type potassium currents in *Xenopus* oocytes. Neuron *1*, 659–667.

Timpe, L. C., Schwarz, T. L., Tempel, B. L., Papazian, D. M., Jan, Y. N., and Jan, L. Y. (1988b). Expression of functional potassium channels from *Shaker cDNA in Xenopus* oocytes. Nature *331*, 143–145.

Trimmer, J. S., Cooperman, S. S., Tomiko, S. A., Zhou, J., Crean, S. M., Boyle, M. B., Kallen, R. G., Sheng, Z., Barchi, R. L., Sigworth, F. J., Goodman, R. H., Agnew, W. S., and Mandel, G. (1989). Primary structure and functional expression of a mammalian skeletal muscle sodium channel. Neuron *3*, 33–49.

Yokoyama, S., Imoto, K., Kawamura, T., Higashida, H., Iwabe, N., Miyata, T., and Numa, S. (1989). Potassium channels from NG-108-15 neuroblastoma-glioma hybrid cells: primary structure and functional expression from cDNAs. FEBS Lett. *259*, 37–42.

Zagotta, W. N., Germeraad, S., Garber, S. S., Hoshi, T., and Aldrich, R. W. (1989a). Properties of *Sh*B A-type potassium channels expressed in *Shaker* mutant Drosophila by germline transformation. Neuron *3*, 773–782.

Zagotta, W. N., Hoshi, T., and Aldrich, R. W. (1989b). Gating of single Shaker potassium channels in Drosophila muscle and in Xenopus oocytes injected with *Shaker* mRNA. Proc. Natl. Acad. Sci. USA *86*, 7243–7247.